MATERIALS CHEMISTRY
FRONTIERS

RESEARCH ARTICLE

View Article Online
View Journal | View Issue

Cite this: *Mater. Chem. Front.*, 2019, **3**, 1793

Reactive oxygen species-responsive theranostic nanoparticles for enhanced hypoxic tumor photodynamic therapy *via* synchronous HIF-1α inhibition and ATP depletion†

Caiyan Zhao,‡[ad] Yunhao Li,‡[b] Leihou Shao,[ad] Xuan Wang,[ad] Jianqin Lu,[a] Xianlei Li,[ad] Long Chen,[ad] Xinyue Cui,[ac] Wang Sheng,*[c] Xiongwei Deng*[a] and Yan Wu*[ad]

A major impediment in photodynamic therapy (PDT) against hypoxic tumors is that the O_2-dependent PDT is seriously limited by the intrinsic hypoxic feature. Hypoxia-inducible factor-1 alpha (HIF-1α) is a key transcription factor in tumor development and especially accumulates in hypoxic tumors and has been recognized as a novel therapeutic target. Herein, we developed small molecule HIF-1α inhibitor Doxy and IR780 photosensitizer co-incorporated methoxy poly(ethylene glycol)-*b*-poly-(propylene sulfide) ($mPEG_{50}$-*b*-PPS_{45}) nanoparticles (NPs/ID) as an ROS-responsive theranostic system designed to enhance PDT efficiency by combining the benefits of anti-HIF-1α therapy and ATP depletion. NPs/ID with reinforced phototherapy response in hypoxic tumors displayed enhanced photocytotoxicity compared to NPs/I that only exhibited the PDT effect. On the other hand, NPs/ID have the capacity to reduce the supply of intracellular ATP and destabilize the intracellular redox homeostasis for enough ROS generation by suppressing the HIF-1α expression, thereby facilitating the therapeutic efficiency of PDT. Significantly, NPs/ID displayed effective tumor targeting and NIR imaging ability and an improved *in vivo* efficacy in a xenograft MDA-MB-231 mouse tumor model compared with bare PDT. These findings demonstrate that the ROS-responsive theranostic NPs/ID with special anti-HIF-1α and ATP depletion behavior represent an attractive approach for overcoming the problems of PDT in hypoxic tumors.

Received 26th April 2019,
Accepted 19th June 2019

DOI: 10.1039/c9qm00270g

rsc.li/frontiers-materials

Introduction

Photodynamic therapy (PDT), as a minimally invasive approach for precise ablation of tumors *via* the cytotoxic reactive oxygen species (ROS) generated from surrounding molecular oxygen (O_2) by light activation of a photosensitizer (PS), has emerged as an attractive treatment modality used in clinical practice.[1–5] At this point, O_2 is an essential component in PDT processes. Tumor hypoxia has been found to promote tumor progression and metastasis, and could decrease therapeutic efficiency including chemotherapy and radiotherapy.[6–9] In particular, O_2-dependent PDT is seriously limited by the hypoxic feature of the tumor sites caused by the rapid progression of tumor cells and abnormal vasculogenesis.[10–12] In addition, PDT may aggravate tumor hypoxia through direct oxygen consumption or indirect vascular damage.[13–15] Consequently, there are bad outcomes that tumor hypoxia would inhibit the therapeutic effects of PDT and in turn PDT would promote cancer hypoxia as a result of a vicious cycle.

Hypoxia-inducible factor-1α (HIF-1α) is a key transcription factor during hypoxia.[16] It activates the transcription of genes that are involved in crucial aspects of cancer biology, including angiogenesis, cell proliferation, metastasis and glucose metabolism.[17,18] HIF-1α-dependent induction of glycolytic genes is considered particularly critical for metabolic adaptation of cells to hypoxia, which involves shifting glucose metabolites from the metabolism through the tricarboxylic acid cycle (TCA) in mitochondria to anaerobic glycolysis, thus increasing ATP production for compensating the hypoxic cellular energy demands.[19] Meanwhile, the metabolic intermediates attenuate hypoxic ROS generation and rescue the cells from hypoxia-induced apoptosis.[20] In addition, HIF-1α could activate the transcription of several metabolic enzymes serving to decrease

[a] *CAS Key Laboratory for Biomedical Effects of Nanomaterials and Nanosafety, CAS Center for Excellence in Nanoscience, National Center for Nanoscience and Technology, Beijing 100190, China. E-mail: dengxw2018@nanoctr.cn, wuy@nanoctr.cn*
[b] *Department of Clinical Medicine, Zhongshan School of Medicine, Sun Yat-sen University, Guangzhou, 510080, China*
[c] *College of Life Science and Bioengineering, Beijing University of Technology, No. 100 Pingleyuan, Beijing 100124, P. R. China. E-mail: shengwang@bjut.edu.cn*
[d] *University of Chinese Academy of Sciences, Beijing 100049, China*
† Electronic supplementary information (ESI) available. See DOI: 10.1039/c9qm00270g
‡ These authors contributed equally to this work.

the production of oxidants and increase the production of antioxidants to maintain the cellular redox homeostasis. Recent studies have demonstrated that the glycolytic enzyme (*e.g.*, fructose-biphosphatase aldolase A) activity is positively correlated with hypoxia inducible factor-1a expression levels in various cancer cells and could be proposed as a new target for the inhibition of HIF-1α activity.[21–27] Doxycycline hyclate (Doxy), a well-known traditional antibiotic drug with broad-spectrum, has the potential to decrease the HIF-1α activity by inducing glycolytic enzyme down-expression or altering cellular metabolism.[28–33]

As an attractive heterogeneity point, cancer cells have ten times higher ROS concentration than normal cells.[34–37] Thus, ROS-responsive nanoparticles have been designed and employed to increase the drug selectivity in cancer cells, thus increasing therapeutic efficacy and decreasing side effects.[38–41] Herein, we aimed to explore using ROS-responsive nanoparticles to co-deliver a small molecule HIF-1α inhibitor Doxy and the photosensitizer IR780 for enhanced PDT efficiency. As shown in Scheme 1, the developed ROS-responsive nanoparticles (NPs/ID) were self-assembled from amphipathic methoxy poly(ethylene glycol)-*b*-poly-(propylene sulfide) ($mPEG_{50}$-*b*-PPS_{45}) block copolymer, in which hydrophilic Doxy and hydrophobic IR780 were simultaneously co-incorporated. The $mPEG_{50}$-*b*-PPS_{45}-based NPs showed good biocompatibility both *in vitro* and *in vivo*. Meanwhile, the PEG component in the NPs could receive improved stability and NPs/ID could accumulate in the tumor site and image the tumor effectively through EPR-based passive targeting ability. After entering cancer cells, the NPs/ID was irradiated with a near-infrared (NIR) laser, which would induce a remarkable increase in the ROS level. Subsequently, the generated ROS would trigger the disassembly of the NPs/ID, leading to enhanced Doxy release. Furthermore, released Doxy would simultaneously inhibit the HIF-1α activity and decrease ATP production in cancer cells, which enhances the therapeutic efficiency by synergizing starvation therapy with PDT. Most surprisingly, Doxy had the capacity to destabilize the cellular redox homeostasis through inhibiting the HIF-1α activity for improved ROS generation, significantly facilitating the therapeutic efficiency of PDT.

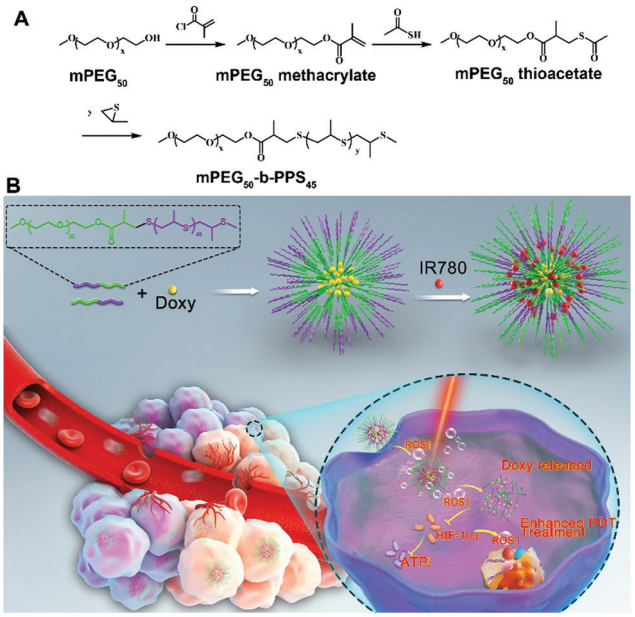

Scheme 1 Schematic illustration of NPs/ID preparation and mechanism of anti-HIF-1α for enhanced PDT against hypoxic tumor. (A) Synthesis route of methoxy poly (ethylene glycol)-*b*-poly(propylene sulfide) ($mPEG_{50}$-*b*-PPS_{45}) copolymer. (B) Schematic of ROS-responsive NPs/ID for enhanced PDT and relative mechanisms.

Results and discussion

We firstly synthesized the amphiphilic $mPEG_{50}$-*b*-PPS_{45} copolymer according to previous reports with some modifications (Scheme 1A).[42] As shown in Fig. S1 (ESI†), the typical ^{1}H NMR spectra results of $mPEG_{50}$-*b*-PPS_{45} were confirmed. The IR780 and Doxy co-incorporated $mPEG_{50}$-*b*-PPS_{45} NPs (NPs/ID) were obtained through the double emulsion technique (w/o/w) method, where hydrophobic IR780 was incorporated in the Oil layer position and hydrophilic Doxy was in the core position (Scheme 1B). As shown in Table S1 (ESI†), as the concentration of $mPEG_{50}$-*b*-PPS_{45} increased, the size and EE% increased as well. The high EE% might result in more effective drug delivery, while the NPs with a larger size were susceptible to elimination through the reticulo-endothelial system (RES). When PVA and pluronic F68 with a ratio of 7 : 3 was used, a smaller size was obtained and this ratio was chosen in our following studies. The average hydrodynamic diameter of the NPs/ID_1 (the IR780 and Doxy with a ratio of 1 : 2) in aqueous solution was determined as 225.6 ± 4.6 nm by dynamic light scattering (DLS) (Fig. 1A). From the transmission electron microscope (TEM) images, the NPs were typical spherical core–shell shape with the size consistent with the DLS measurement (Fig. 1A). It also showed that no significant change of NPs/ID_1 was observed for up to 7 days (Fig. 1B), indicating the good stability of the NPs. The UV-vis absorption spectrum of NPs/I (NPs only loaded with IR780), NPs/ID_1, or NPs/ID_2 (the IR780 and Doxy with a ratio of 1 : 5) in aqueous solution displayed the same maximum absorption at about 800 nm (Fig. S2, ESI†). The photostability of organic dyes played a fundamental role in biomedical applications. So we measured the fluorescence spectra of free IR780, NPs/I, and NPs/ID_1 storage for different times. As shown in Fig. S3 (ESI†), the fluorescence intensity (FI) of NPs/I and NPs/ID_1 only exhibited a slight reduction after storage for 5 days, demonstrated that these nanoparticles had excellent photostability.

Next, singlet oxygen sensor green (SOSG) was used to detect $^1O_2$ generation, whose fluorescence was quenched in its original state, but its fluorescence could be recovered once it had been oxidized by $^1O_2$. As shown in Fig. 1C, the fluorescence intensity of SOSG in NPs/I, NPs/ID_1 or NPs/ID_2 solution increased consistently upon NIR light irradiation under normal oxygen conditions (NC), indicating that $^1O_2$ was efficiently produced. In comparison, the FI in all groups turned relatively weak under hypoxic conditions (HC), indicating that the HC environment with a reduced oxygen content would inhibit the ROS generation greatly.

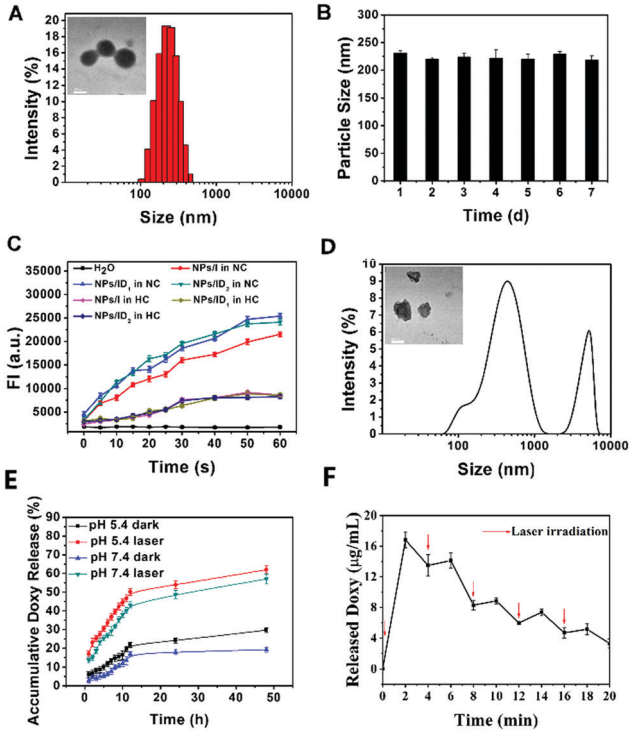

Fig. 1 Characterization of nanoparticles. (A) Size distribution of NPs/ID_1 measured by DLS. The inset shows the TEM image of NPs/ID_1. Scale bar: 100 nm. (B) Particle size changes during 7 days measured by DLS. (C) *In vitro* $^1O_2$ generation of NPs/I, NPs/ID_1 and NPs/ID_2 under NIR laser irradiation (808 nm laser, 2 W cm^{-2}) under normal conditions (NC) or hypoxic conditions (HC) for a continuous time. (D) Size distribution of NPs/ID_1 at 4 h after NIR laser irradiation (808 nm laser, 2 W cm^{-2}). The inset showed the relative TEM image. Scale bar: 100 nm. (E) *In vitro* accumulative release of Doxy from NPs/ID_1 under different conditions. (F) Pulsatile release profile of NPs/ID_1 both in the dark and under NIR laser irradiation.

Then, the ROS-responsive behaviour of NPs/ID was investigated (Fig. 1D). After NIR light irradiation within 2 min and incubation for another 4 h, the size distribution and the corresponding morphology of the NPs/ID_1 changed greatly. The DLS results indicated that the NPs/ID_1 obviously swelled and dissociated after NIR light irradiation. The TEM observation also showed that the spherical core–shell structure of NPs/ID_1 collapsed and became irregular. These phenomena implied the disassembly of the NPs. Under oxidative conditions, the PPS component could degrade to the polysulfoxide and finally became hydrophilic polysulfone, thus altering its original hydrophobicity and acting as an ROS-responsive system. Subsequently, the ROS-triggered release behaviour of Doxy from NPs/ID_1 was investigated. After incubation in PBS solution for 48 h, approximately 57% or 62% of Doxy could be released for the NPs/ID_1 treated with laser treatment both at pH 7.4 or pH 5.4, whereas only 19% of Doxy was released for the NPs/ID_1 at pH 7.4 without laser treatment (Fig. 1E). Moreover, the Doxy from NPs/ID_1 presented a pulsatile release pattern when it was alternatively exposed to NIR light or kept in the dark every 2 min for several cycles (Fig. 1F). These results demonstrated the ROS-responsive

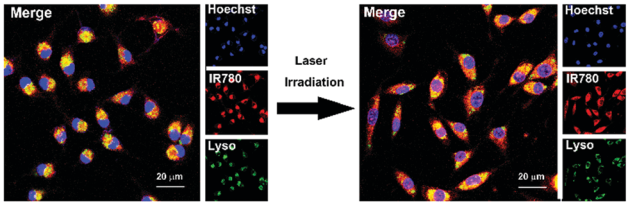

Fig. 2 Intracellular distribution of NPs/ID_1 observed by CLSM. The endosomes and lysosomes were stained by LysoTracker Green, and the nuclei were stained by Hoechst 33342. (The left group was without NIR laser irradiation; right was with NIR laser irradiation (808 nm, 2 W cm^{-2}).)

behaviour of NPs/ID and the ROS-triggered release of Doxy from NPs/ID under laser treatment.

We next evaluated the cellular uptake and Doxy release behaviour of NPs/ID in MDA-MB-231 cells. As shown in Fig. 2, for the cells without laser irradiation treatment, the fluorescence of IR780 (red) was mainly co-localized with endo/lysosomes stained by LysoTracker (green). In contrast, after the 808 nm laser irradiation, obvious fluorescence could also be observed inside both the cell cytoplasm and nucleus, suggesting that the produced ROS *via* the PDT effect could induce the disassembly of NPs/ID and facilitate endosomal escape and drug release. Subsequently, the 3-[4,5-dimethyl-thiazol-2-yl]-2,5-diphenyl-tetrazolium bromide (MTT) assay was used to investigate the cytotoxicity of blank NPs against normal 3T3 cells or HUVEC cells to avoid the toxicity caused by drug carriers. As shown in Fig. S4 (ESI†), the cell survival rate was greater than 80% even after treatment with drug-free NPs at a high concentration of 500 μg mL^{-1}, demonstrating that the prepared NPs had preferable biocompatibility. To assess the potential enhanced PDT efficiency of Doxy in NPs/ID under a hypoxia environment, the MDA-MB-231 cells were pre-treated with $CoCl_2$ (100 mM) to induce hypoxia. Then, the cells were incubated with NPs/I, NPs/I + $Doxy_1$ and NPs/I + $Doxy_2$ (IR780, 0–10 μg mL^{-1}) for 24 h and the cell cytotoxicity was evaluated by MTT assay (Fig. S5, ESI†). The cells incubated with NPs/I under normoxia conditions were used as a control. As expected, the NPs/I-treated cells exhibited effective cytotoxicity in normoxia conditions under laser irradiation and exhibited a concentration and laser power dependent manner, whereas relatively weak toxicity was observed under hypoxic conditions. In contrast, the combination of Doxy and NPs/I showed significant cytotoxicity in hypoxia to the cancer cells. Compared to NPs/I, the NPs/I + $Doxy_1$ and NPs/I + $Doxy_2$ were more toxic in hypoxia. Furthermore, the cells were incubated with NPs/I, NPs/ID_1, NPs/ID_2, $Doxy_1$, or $Doxy_2$ in hypoxia (IR780, 5 μg mL^{-1}) (Fig. 3A and B). The cells treated with only NIR light or different NP formulations without laser irradiation did not show a significant decrease of viability, also implying the negligible toxicity of all NPs. However, the cells treated with NPs/I, NPs/ID_1 and NPs/ID_2 in combination with NIR irradiation showed obvious cytotoxic effects. In addition, the cytotoxicity increased along with the Doxy concentration and incubation time.

Consistent with the above MTT results, nearly no cell death was observed for the untreated group or Doxy treatment groups with the fluorescence live/dead cell staining assay (Fig. 3C).

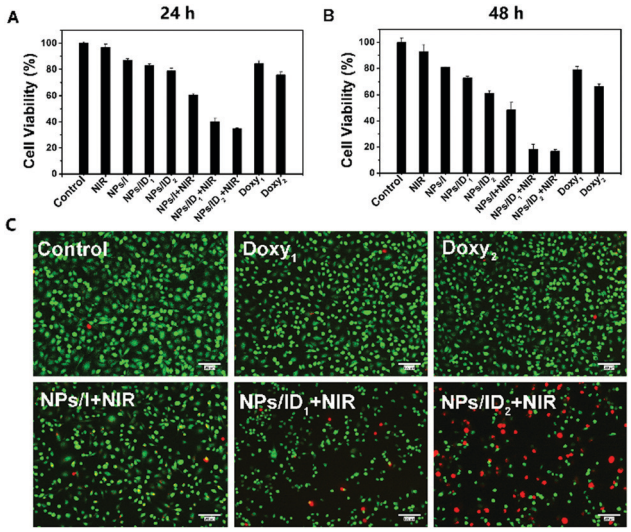

Fig. 3 (A and B) *In vitro* cytotoxicity of MDA-MB-231 cells treated for 24 h or 48 h with NIR, NPs/I, NPs/ID_1, NPs/ID_2, NPs/I + NIR laser, NPs/ID_1 + NIR laser, NPs/ID_2 + NIR laser, $Doxy_1$, or $Doxy_2$. (C) Fluorescent images of MDA-MB-231 cells with a Live-Dead Cell Staining Kit staining after various treatments. The NIR laser was 808 nm, 1 W cm^{-2}. Scale bar: 100 μm.

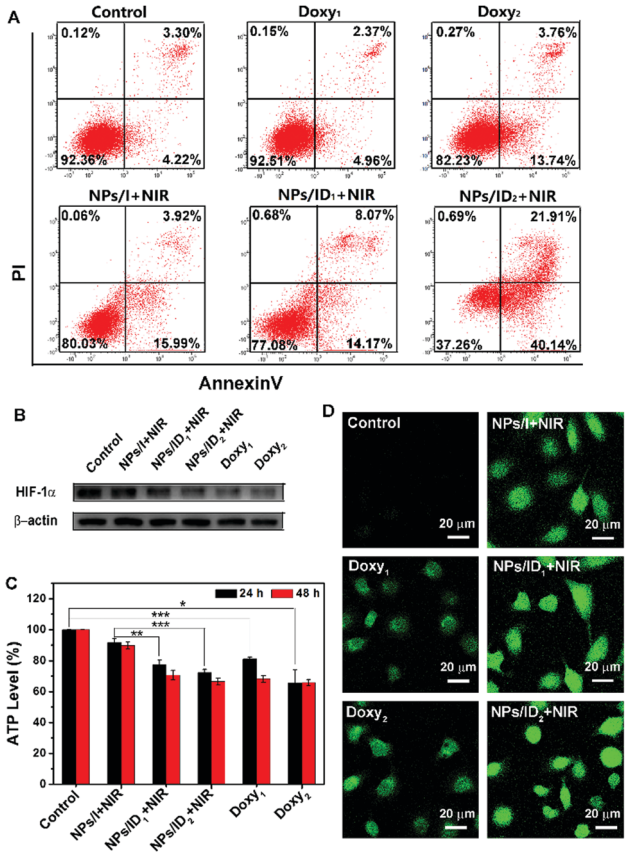

Fig. 4 (A) Flow cytometry analysis of MDA-MB-231 cell apoptosis after treatment with various formulation for 24 h. (B) Western-blot analysis. (C) ATP content in MDA-MB-231 cells detected by ATPlite Assay Kit. (D) ROS generation in MDA-MB-231 cells after treatment with different formulations.

After being treated with NPs/I and laser irradiation, some dead cells with red fluorescence were observed. In contrast, the NPs/ID_1 induced more efficient cell death under the same irradiation conditions. And the number of dead cells increased after being treated with NPs/ID_2 as the concentration of the Doxy increased. Furthermore, an Annexin V-FITC/PI apoptosis assay was performed by flow cytometry. As shown in Fig. 4A, the quantitative results verified the improved cell apoptotic efficacy of both cells treated with NPs/ID_1 and NPs/ID_2 under hypoxia conditions. In particular, the NPs/ID_2 treatment showed the highest apoptotic ratio of 62.05% (the early apoptotic ratio of 40.14%, the late apoptotic ratio of 21.91%). These conclusions suggested that the Doxy could enhanced IR780-mediated PDT cytotoxicity under hypoxia conditions.

The Western-blot analysis was then performed to detect the expression of HIF-1α in the hypoxic cells treated with $Doxy_1$, $Doxy_2$ and NPs/I, NPs/ID_1, and NPs/ID_2 plus irradiation. As expected, an up-regulated level of HIF-1α could be detected in hypoxic MDA-MB-231 cells. With $Doxy_1$, $Doxy_2$, NPs/ID_1, or NPs/ID_2 treatment, the expression of HIF-1α in hypoxic cells was effectively inhibited and the level of HIF-1α gradually decreased with increasing concentration of the Doxy. However, the NPs/I did not cause the down-regulation of the HIF-1α expression (Fig. 4B). It was supposed that the introduction of Doxy into NPs/ID could effectively down-regulate the expression level of HIF-1α in hypoxic tumor cells. Next, we continued to explore if the released Doxy from NPs/ID could influence the ATP production in hypoxic MDA-MB-231 cells after down-regulating the expression of HIF-1α. As shown in Fig. 4C, compared with the untreated group, there was 18.76, 34.25, 22.69, and 27.58% reduction of the ATP level in cells after being treated with $Doxy_1$, $Doxy_2$, NPs/ID_1 and NPs/ID_2 for 24 h, respectively. After being treated for 48 h, more serious reduction of the intracellular ATP level was detected. In contrast, the NPs/I treatment had almost no influence on the intracellular ATP level. These results demonstrated that the Doxy not only could down-regulate HIF-1α expression, but also could inhibit the cellular ATP production and disturb the cancer cell energy supply, which was complementary to the PDT against hypoxic tumor cells. As a result, the cancer cells were more sensitive to the damage induced by PDT.

In addition, we utilized the 2′,7-dichlorodihydrofluorescein diacetate (DCFH-DA) probe to evaluate the ROS generation under NIR irradiation in hypoxic cancer cells. Surprisingly, the results showed that the Doxy induced the enhancement of the ROS level in cells with slight DCF fluorescence observation, and the DCF fluorescence became brighter as the Doxy concentration increased. For the cells treated with NPs/I plus irradiation, the DCF fluorescence looked relatively weaker than that treated with NPs/ID under the same irradiation conditions (Fig. 4D). Furthermore, qualitative analysis showed that the generated ROS level in cells treated with NPs/ID_1 or NPs/ID_2 is increased about 33.44% or 45.29% of that in cells with incubation of NPs/I, respectively. After extending the incubation time to 6 h, the NPs/ID-treated cells showed stronger fluorescence intensity. The NPs/ID_1-treated cells improved approximately

1.8 times in fluorescence intensity and the NPs/ID_2 improved approximately 1.9 times as compared with NPs/I (Fig. S6, ESI†).

Subsequently, NIR fluorescence imaging-guided whole-body biodistribution of NPs/ID was evaluated in tumor-bearing nude mice by intravenous injection of NPs/ID_1. As shown in Fig. 5A, enhanced fluorescence could be observed at the tumor site relative to other normal regions for NPs/ID_1-treated mice from 3 h to 24 h post injection, whereas weak fluorescence was found for naked IR780-treated mice throughout the whole body. The *ex vivo* fluorescent imaging on major organs also demonstrated that the NPs/ID_1 were predominantly accumulated in the tumor site (Fig. S7, ESI†). These results demonstrated that NIR fluorescence of NPs/ID_1 could also be used to image the tumor effectively. Next, we evaluated the anti-HIF-1α activity *in vivo*. According to Fig. 5B, bright green fluorescence could be observed in the untreated group, indicating the high expression of HIF-1α. While reduced HIF-1α immunofluorescence was displayed after treatment with $Doxy_1$, $Doxy_2$, NPs/ID_1 or NPs/ID_2, illustrating that Doxy and Doxy containing NPs could decrease the expression of HIF-1α. Western-blot assays were in accordance with the above result (Fig. 5C). In addition, consistent with the results at a cellular level, the ATP levels in the groups treated with Doxy or NPs/ID were significantly down-regulated, but slightly up-regulated after treatment with NPs/I (Fig. 5D). Compared with the untreated group, the ROS level increased about 1.57 times in the NPs/I treatment group, while the ROS level increased about 2.38 times for NPs/ID_1 treatment and 2.88 times for NPs/ID_2 treatment, respectively (Fig. 5E). These results further confirmed that the ROS generation was in negative correlation with the HIF-1α expression and the level of ATP.

Finally, the *in vivo* antitumor efficacy of NPs/ID was studied in an MDA-MB-231 xenograft mouse model. As illustrated in Fig. 6A, the free Doxy, NPs/ID_1, or NPs/ID_2 exhibited only moderate anticancer activity and NPs/I plus laser irradiation displayed a certain tumor growth suppression. Of note, the tumor was remarkably suppressed after treatment with NPs/ID_1, or NPs/ID_2 plus laser irradiation due to the combination of PDT with the metabolism disturbances and the therapeutic efficacy exhibited Doxy does-reliable improvement. In addition, the body weights of NPs/ID-treated mice exhibited a similar manner to that of the control group (Fig. 6B). The corresponding tumor weight (Fig. 6C) and tumor photograph (Fig. 6D) from sacrificed mice at 15 days post-injection also demonstrated the higher therapeutic efficacy of NPs/ID formulations. Furthermore, severe tissue necrosis was observed from tumor sections by hematoxylin and eosin (H&E) staining in the NPs/ID_2 and laser treatment group (Fig. 6E). These results strongly suggested the excellent anticancer efficacy of NPs/ID. No significant physiological morphology changes were observed in the main organs after treatment with various drug formulations compared to the control group, suggesting the good biocompatibility of NPs/ID for biological applications (Fig. S8, ESI†).

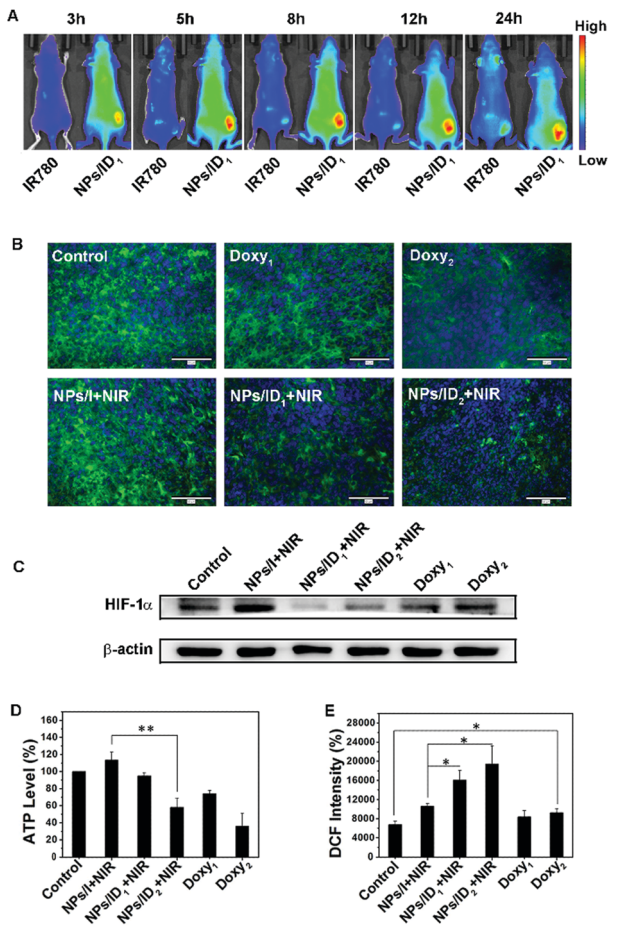

Fig. 5 (A) *In vivo* fluorescence images of mice at 3, 5, 8, 12, and 24 h after intravenous injection of free IR780 or NPs/ID_1. (B) Immunofluorescence staining images of tumors treated with various formulations. The hypoxic section was visualized by HIF-1α staining (green), and the cell nuclei were stained with DAPI (blue). Scale bar: 50 μm. (C) HIF-1α expression of tumors detected by Western-blot. (D and E) ATP content and ROS generation in tumors after treatment with various formulations.

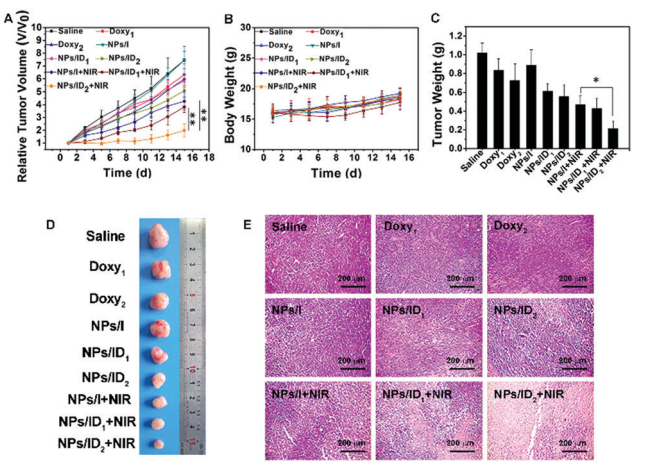

Fig. 6 (A) Tumor growth curves in mice treated with various formulations. (B) Mouse body weight changes of different groups over the course of the treatments. (C) The tumor weight of different groups calculated at time of sacrifice. (D) Representative images of the tumors of different groups at time of sacrifice. (E) Representative H&E sections of tumor tissue of different groups. The values are expressed as mean ± SD, (n = 5).

Conclusions

In conclusion, small molecule HIF-1α inhibitor Doxy and photosensitizer IR780 co-incorporated NPs/ID as an ROS-responsive system was successfully developed to enhance PDT sensitization in hypoxic tumors by combining the benefits of anti-HIF-1α and ATP depletion strategies. NPs/ID with reinforced phototherapy response in hypoxic tumors displayed enhanced photocytotoxicity compared to NPs/I that only exhibited the PDT effect. NPs/ID have the capacity to reduce the supply of intracellular ATP and destabilize the intracellular redox homeostasis for enough ROS generation by suppressing the HIF-1α expression, thereby facilitating the therapeutic efficiency of PDT. In addition, NIR fluorescence of NPs/ID_1 could be used to image the tumour effectively. Collectively, the established NPs/ID nanoparticles had a great potential to be used as an ROS-responsive theranostic platform with excellent biocompatibility for inhibition of HIF-1α expression and ATP level and enhanced PDT strategy against hypoxic tumors.

Conflicts of interest

There are no conflicts to declare.

Acknowledgements

We are grateful for the financial support of the following programmes: The National Natural Science Foundation of China (Grant No. 81773185, 81472850 and 81502288).

Notes and references

1 J. F. Lovell, T. W. B. Liu, J. Chen and G. Zheng, *Chem. Rev.*, 2010, **110**, 2839.
2 Z. J. Zhou, J. B. Song, L. M. Nie and X. Y. Chen, *Chem. Soc. Rev.*, 2016, **45**, 6597–6626.
3 D. E. J. G. J. Dolmans, D. Fukumura and R. K. Jain, *Nat. Rev. Cancer*, 2003, **3**, 380–387.
4 Q. Wang, B. Xia, J. Xu, X. Niu, J. Cai, Q. Shen, W. Wang, W. Huang and Q. Fan, *Mater. Chem. Front.*, 2019, **3**, 650–655.
5 Q. Wang, P. Zhang, J. Xu, B. Xia, L. Tian, J. Chen, J. Li, F. Lu, Q. Shen, X. Lu, W. Huang and Q. Fan, *ACS Appl. Bio Mater.*, 2018, **1**, 70–78.
6 T. S. Lin, X. Z. Zhao, S. Zhao, H. Yu, W. M. Cao, W. Chen, H. Wei and H. Q. Guo, *Theranostics*, 2018, **8**, 990–1004.
7 H. Cheng, J. Y. Zhu, S. Y. Li, J. Y. Zeng, Q. Lei, K. W. Chen, C. Zhang and X. Z. Zhang, *Adv. Funct. Mater.*, 2016, **26**, 7847–7860.
8 L. Cheng, C. Wang, L. Z. Feng, K. Yang and Z. Liu, *Chem. Rev.*, 2014, **114**, 10869–10939.
9 Q. Wang, L. Tian, J. Xu, B. Xia, J. Li, F. Lu, X. Lu, W. Wang, W. Huang and Q. Fan, *Chem. Commun.*, 2018, **54**, 10328–10331.
10 Y. Dai, C. Xu, X. Sun and X. Chen, *Chem. Soc. Rev.*, 2017, **46**, 3830–3852.
11 W. Fan, P. Huang and X. Chen, *Chem. Soc. Rev.*, 2016, **45**, 6488–6519.
12 W. Wilson and M. Hay, *Nat. Rev. Cancer*, 2011, **11**, 393–410.
13 W. M. Gallagher, L. T. Allen, C. O'Shea, T. Kenna, M. Hall, A. Gorman, J. Killoran and D. F. O'Shea, *Br. J. Cancer*, 2005, **92**, 1702.
14 X. L. Cai, Y. A. Luo, Y. Song, D. Liu, H. Y. Yan, H. Li, D. Du, C. Z. Zhu and Y. H. Lin, *Nanoscale*, 2018, **10**, 22937–22945.
15 Z. Lv, H. J. Wei, Q. Li, X. L. Su, S. J. Liu, K. Y. Zhang, W. Lv, Q. Zhao, X. H. Li and W. Huang, *Chem. Sci.*, 2018, **9**, 502–512.
16 D. Samanta and G. L. Semenza, *Cancer Res.*, 2016, **76**, 1–5.
17 G. L. Semenza, *BBA, Biochim. Biophys. Acta, Mol. Cell Res.*, 2016, **1863**, 382–391.
18 S. Koyasu, M. Kobayashi, Y. Goto, M. Hiraoka and H. Harada, *Cancer Sci.*, 2018, **109**, 560–571.
19 J.-w. Kim, I. Tchernyshyov, G. L. Semenza and C. V. Dang, *Cell Metab.*, 2006, **3**, 177–185.
20 P. Carmeliet, Y. Dor, J.-M. Herbert, D. Fukumura, K. Brusselmans, M. Dewerchin, M. Neeman, F. Bono, R. Abramovitch, P. Maxwell, C. J. Koch, P. Ratcliffe, L. Moons, R. K. Jain, D. Collen and E. Keshet, *Nature*, 1998, 394–485.
21 Y.-C. Chang, Y.-C. Chan, W.-M. Chang, Y.-F. Lin, C.-J. Yang, C.-Y. Su, M.-S. Huang, A. T. H. Wu and M. Hsiao, *Cancer Lett.*, 2017, **403**, 28–36.
22 Z. H. Jiang, X. H. Wang, J. Li, H. M. Yang and X. Lin, *J. Cell. Mol. Med.*, 2018, **22**, 4377–4386.
23 G. L. Semenza, *Trends Pharmacol. Sci.*, 2012, **33**, 207–214.
24 I. F. Robey, A. D. Lien, S. J. Welsh, B. K. Baggett and R. J. Gillies, *Neoplasia*, 2005, **7**, 324–330.
25 M. Lee, J. Hwang, H. Lee, S. Jung, I. Kang, S. Chi, S. Kim and J. Ha, *J. Biol. Chem.*, 2003, **278**, 39653–39661.
26 G. Grandjean, P. R. De Jong, B. P. James, M. Y. Koh, R. Lemos, J. Kingston, A. Aleshin, L. A. Bankston, C. P. Miller and E. J. Cho, *Cancer Res.*, 2016, **76**, 4259–4269.
27 C. T. Taylor, *Biochem. J.*, 2008, **409**, 19–26.
28 Y. Singh, A. Srinivas, M. Gangwar, J. G. Meher, S. Misra-Bhattacharya and M. K. Chourasia, *Mol. Pharmaceutics*, 2016, **13**, 2084–2094.
29 G. L. Semenza, *Curr. Pharm. Des.*, 2009, **15**, 3839–3843.
30 E. M. D. Francesco, M. Maggiolini, H. B. Tanowitz, F. Sotgia and M. P. Lisanti, *Oncotarget*, 2017, **8**, 56126–56142.
31 R. Lamb, M. Fiorillo, A. Chadwick, B. Ozsvari, K. J. Reeves, D. L. Smith, R. B. Clarke, S. J. Howell, A. R. Cappello and U. E. Martinez-Outschoorn, *Oncotarget*, 2015, **6**, 14005.
32 J. H. Um, C. D. Kang, J. H. Bae, G. G. Shin, D. W. Kim, B. S. Chung and S. H. Kim, *Exp. Mol. Med.*, 2004, **36**, 233.
33 E. Ahler, W. J. Sullivan, A. Cass, D. Braas, A. G. York, S. J. Bensinger, T. G. Graeber and H. R. Christofk, *PLoS One*, 2013, **8**, 64561.
34 D. Trachootham, J. Alexandre and P. Huang, *Nat. Rev. Drug Discovery*, 2009, **8**, 579–591.
35 R. Li and Y. Xie, *J. Controlled Release*, 2017, **251**, 49–67.
36 Z. B. Li, M. Wu, H. Z. Bai, X. G. Liu and G. Tang, *Chem. Commun.*, 2018, **54**, 13127–13130.

37 X. M. Lv, Y. Y. Zhu, H. Ghandehari, A. Yu and Y. J. Wang, *Chem. Commun.*, 2019, **55**, 3383–3386.
38 D. Q. Chen, G. Q. Zhang, R. M. Li, M. R. Guan, X. Y. Wang, T. J. Zou, Y. Zhang, C. R. Wang, C. Y. Shu, H. Hong and L. J. Wan, *J. Am. Chem. Soc.*, 2018, **140**, 7373–7376.
39 X. Y. Zhang, L. Han, M. Y. Liu, K. Wang, L. Tao, Q. Wang and Y. Wei, *Mater. Chem. Front.*, 2017, **1**, 807–822.
40 W. H. Wang, G. H. Liang, W. J. Zhang, D. Xing and X. L. Hu, *Chem. Mater.*, 2018, **30**, 3486–3498.
41 Y. Dai, J. Su, K. Wu, W. Ma, B. Wang, M. Li, P. Sun, Q. Shen, Q. Wang and Q. Fan, *ACS Appl. Mater. Interfaces*, 2019, **11**, 10540–10553.
42 H. Deng, X. Zhao, L. Deng, J. Liu and A. Dong, *J. Controlled Release*, 2017, **255**, 142–153.